Molecular Features of an Alcohol Binding Site in a Neuronal Potassium Channel†

Mohammad Shahidullah,‡ Thanawath Harris,‡ Markus W. Germann,§ and Manuel Covarrubias*,‡

Department of Pathology, Anatomy and Cell Biology, Jefferson Medical College of Thomas Jefferson University, 1020 Locust Street, Philadelphia, Pennsylvania 19107, and Department of Chemistry, Georgia State University, University Plaza, Atlanta, Georgia 30303

Received May 7, 2003; Revised Manuscript Received June 25, 2003

ABSTRACT: Aliphatic alcohols (1-alkanols) selectively inhibit the neuronal Shaw2 K^+ channel at an internal binding site. This inhibition is conferred by a sequence of 13 residues that constitutes the S4−S5 loop in the pore-forming subunit. Here, we combined functional and structural approaches to gain insights into the molecular basis of this interaction. To infer the forces that are involved, we employed a fast concentration-clamp method (10−90% exchange time = 800 μs) to examine the kinetics of the interaction of three members of the homologous series of 1-alkanols (ethanol, 1-butanol, and 1-hexanol) with Shaw2 K^+ channels in *Xenopus* oocyte inside-out patches. As expected for a second-order mechanism involving a receptor site, only the observed association rate constants were linearly dependent on the 1-alkanol concentration. While the alkyl chain length modestly influenced the dissociation rate constants (decreasing only ∼2-fold between ethanol and 1-hexanol), the second-order association rate constants increased *e*-fold per carbon atom. Thus, hydrophobic interactions govern the probability of productive collisions at the 1-alkanol binding site, and short-range polar interactions help to stabilize the complex. We also examined the relationship between the energetics of 1-alkanol binding and the structural properties of the S4−S5 loop. Circular dichroism spectroscopy applied to peptides corresponding to the S4−S5 loop of various K^+ channels revealed a correlation between the apparent binding affinity of the 1-alkanol binding site and the α-helical propensity of the S4−S5 loop. The data suggest that amphiphilic interactions at the Shaw2 1-alkanol binding site depend on specific structural constraints in the pore-forming subunit of the channel.

Alcohol and general anesthetic agents interact with related and relatively specific binding sites in multiple protein targets (*1*−*6*). Aliphatic alcohols (e.g., 1-alkanols) have been used to probe the physicochemical properties of these binding sites (*7*−*11*). The results of these studies are consistent with the presence of physically circumscribed hydrophobic protein cavities that constitute the alcohol and general anesthetic sites. Also, studies with soluble model proteins have examined the relationship between anesthetic solubility and anesthetic action along with structure−function analysis and thermodynamic arguments and suggest that polar interactions also contribute to the binding of alcohol and inhaled anesthetics (*5*, *9*, *12*−*15*). Polar interactions are also likely to contribute to the binding of general anesthetic agents to ion channels, which are critical physiological targets of these agents (including 1-alkanols). Our earlier work has shown that the *Drosophila* Shaw2 K^+ channel is a robust model for investigating the protein-based theories of alcohol intoxication and general anesthetic action (*16*−*18*). Shaw2 K^+ channels are members of the superfamily of voltage-gated K^+ channels (Kv channels). Pharmacologically relevant concentrations of 1-alkanols selectively inhibit the Shaw2 K^+ channel by stabilizing the closed state at an internal site, which is probably determined by the 13-amino acid sequence that constitutes the internal S4−S5 loop in the pore-forming subunit of the channel (*16*−*20*). Between ethanol and 1-hexanol, the apparent equilibrium dissociation constants decrease with the 1-alkanol carbon chain length according to the Meyer−Overton rule (*17*, *18*). The binding free energy change per methylene group (−3 kJ/mol) corresponds to the free energy change necessary to transfer 1-alkanols from water to alkanes (*21*, *22*). With longer chain 1-alkanols (longer than 1-heptanol), the binding free energy change levels off. Thus, as expected for the interaction of general anesthetic agents with their targets, a hydrophobic effect at a circumscribed site plays a significant role in the inhibition of Shaw2 K^+ channels by 1-alkanols. However, it is not clear how the hydrophobic effect and the predicted polar interactions control the kinetics of 1-alkanol binding. Also, although the S4−S5 loop in the Shaw2 K^+ channel clearly confers the inhibition by 1-alkanols, it is not known what structural features of this segment are responsible for this unique response.

Here, we employed a combination of functional and structural approaches to shed some light on the solutions to these problems. Using a fast solution exchange system (concentration-clamp), we investigated the kinetics of the inhibition of Shaw2 K^+ channels by ethanol, 1-butanol, and

† This work was supported by a research grant form the National Institutes of Health (NIH) to M.C. (R01-AA10615). M.S. was supported by a training grant from the NIH (AA07463).

* To whom correspondence should be addressed: Department of Pathology, Anatomy and Cell Biology, Jefferson Medical College of Thomas Jefferson University, 1020 Locust St., Philadelphia, PA 19107. Telephone: (215) 503-4341. Fax: (215) 923-2218. E-mail: manuel.covarrubias@jefferson.edu.

‡ Jefferson Medical College of Thomas Jefferson University.

§ Georgia State University.

10.1021/bi034738f CCC: $25.00
Published on Web 08/30/2003

1-hexanol. All three 1-alkanols exhibited second-order binding kinetics, which allowed the estimation of the second-order association rate constants and the dissociation rate constants. From the analysis of the relationship between alkyl chain length and the binding and unbinding rate constants, we inferred the main forces that control the interaction between the Shaw2 K^+ channel and 1-alkanols. Then, the analysis of several peptides corresponding to the S4−S5 loop by CD[1] spectroscopy revealed a relationship between the apparent binding affinity and the α-helical propensity. The observations are discussed in terms of a working hypothesis, whereby hydrophobic and weak short-range polar forces help to determine the extent of binding of 1-alkanols to a relatively specific internal site that is constrained by the secondary structure of the S4−S5 loop in the pore-forming subunit of the Shaw2 K^+ channel.

MATERIALS AND METHODS

Molecular Biology and Site-Directed Mutagenesis. cDNAs encoding wild-type or mutant Shaw2 are maintained as previously described (*17*). All mutations were created using QuickChange (Stratagene, La Jolla, CA) according to the manufacturer's specifications and as described previously (*23*), and were confirmed by automated sequencing (Nucleic Acid Facility, Jefferson Cancer Institute, Philadelphia, PA). The Kv1.3 cDNA was a gift from C. Deutsch (University of Pennsylvania, Philadelphia, PA). The creation of chimeric K^+ channels Shaw2-SK and Kv3.4-KS has been described previously (*18*). Capped cRNA for expression in *Xenopus* oocytes was produced by in vitro transcription using the Message Machine Kit (Ambion, Austin, TX).

Oocyte Injection and Electrophysiology. cRNA encoding Shaw2-F335A (see Results) was injected into defolliculated *Xenopus* oocytes (∼5−50 ng/cell) using a Nanoject microinjector (Drummond, Broomall, PA). Currents were recorded 3−7 days postinjection. The Shaw2-F335A mutant was preferred for the experiments reported here because it exhibits higher expression levels and no significantly affected biophysical properties and inhibition by 1-alkanols (*24*). Patch-clamp recording was conducted as described previously (*25*) using an Axopatch 200B apparatus (Axon Instruments, Foster City, CA). Patch pipets were constructed from Corning glass 7052 (Warner Instrument Corp., Hamden, CT). Typically, for macropatch recording, the tip resistance of the recording pipets in the bath solution (see below) was 0.5−1 MΩ. The pipet solution (external) contained 96 mM NaCl, 2 mM KCl, 1.8 mM $CaCl_2$, 1 mM $MgCl_2$, and 5 mM HEPES (pH 7.4, adjusted with NaOH). All experiments were conducted with inside-out patches. The bath solution (internal) contained 98 mM KCl, 1 mM EGTA, 0.5 mM $MgCl_2$, and 10 mM HEPES (pH 7.3, adjusted with KOH). All patch-clamp experiments were carried out at room temperature (22 ± 1 °C).

Concentration-Clamp. For rapid solution exchange experiments with inside-out macropatches, the Shaw2-F335A current was evoked by a 400 ms step depolarization to 50 mV from a holding potential of −100 mV. In some instances, this current exhibits slow inactivation that reduces the current by ∼10% by the end of the 400 ms depolarization. The currents were low-pass-filtered at 1.5 kHz (−3 db, eight-pole Bessel filter; Frequency Devices, Haverhill, MA) and digitized at 5 kHz. Control and 1-alkanol solutions were simultaneously delivered from the thinned tip of a θ capillary tube (100 μm diameter and 8 μm septum) by a gravity-driven system. Both solutions flow constantly during an experiment (flow rate of 4 μL/s) creating a sharp interface (<2 μm) between the two streams. The patch pipet tip exposing the cytoplasmic face of an inside-out patch is positioned in front of the θ tube, about 100 μm from the tip. To accomplish rapid solution exchange, the sharp solution interface is moved by means of a piezoelectric translator (LSS-3100, Burleigh Instruments, Fishers, NY) that controls the position of the θ tube. A typical 100 ms concentration jump started 140 ms after the onset of the depolarization to 50 mV. The solution switching time ($T_{10-90\%}$ is the 10−90% rise time) was estimated to be ∼500 μs by measuring the current elicited by a change in the liquid junction potential at the open tip of a patch pipet. In inside-out oocyte macropatches expressing Kv1.3 channels, we delivered a K^+ concentration jump (from 98 mM to 49 mM to 98 mM) to determine the actual solution exchange time (Figure 1A,B). This response was rapid ($T_{10-90\%}$ = 800 μs) and symmetrical, and the ON and OFF phases were described well by assuming an exponential function (Figure 1). From 12 independent patches, the time constants were 329 ± 14 and 324 ± 19 μs for the ON and OFF phases, respectively (Figure 1C). All calibrations and experiments were conducted with the same θ tube. Generally, the average of 70−100 ON/OFF sweeps was stored for later analysis. Further processing and analysis of these records are described below.

Data Acquisition, Analysis, and Theoretical Computations. Voltage-clamp protocols, the piezoelectric translator, and data acquisition were controlled by a Pentium class computer interfaced with a 12-bit A/D converter (Digidata 1200B using pClamp 8.0, Axon Instruments). Data analysis and curve fitting were conducted using Clampfit (pClamp 9.0, Axon Instruments), Sigmaplot 8.0 (SPSS, Inc., San Rafael, CA), or Origin 7.0 (Origin Lab Inc., Northhampton, MA). All time-dependent current relaxations were described by assuming the exponential function $I(t) = A \exp(-t/\tau) + mt + C$, where $I(t)$ is the current at time t, A is the amplitude of the exponential term, τ is the time constant, m is the slope of a straight line that approximates the slow current decay caused by inactivation (see above), and C is the constant term. The equilibrium dose−inhibition curves were also obtained from the concentration-clamp experiments. At the end of the concentration jump (∼10 sample points), the normalized steady-state level of inhibition was computed as $100(\Delta I/B_{max})$, where $\Delta I = I_{control} - I_{alkanol}$ ($I_{control}$ is the estimated current level in the absence of drug and $I_{alkanol}$ the current level in the presence of drug) and B_{max} is the maximum level of inhibition estimated from each experiment using the Hill equation $\Delta I = B_{max}\{1/[1 + (K_{0.5}/[A])^n]\}$, where $K_{0.5}$ is the apparent equilibrium constant, [A] is the 1-alkanol concentration, and n is the Hill coefficient. Unless indicated otherwise, all pooled values are expressed as the mean ± the standard error.

In concentration-clamp experiments, the finite exchange time of the rapid solution exchange system ($T_{10-90\%}$ = 800 μs) may cause distortion of the current kinetics. We employed the following procedure to eliminate the "blurring" effect of the solution exchange process. Given the symmetric

[1] Abbreviations: CD, circular dichroism; TFE, 2,2,2-trifluoroethanol.

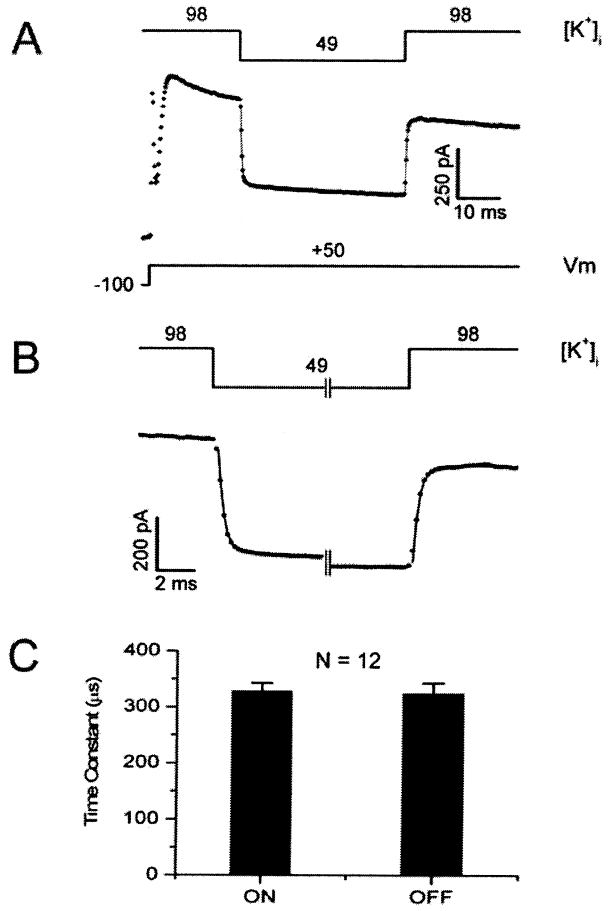

FIGURE 1: Exchange time of a solution switching system applied to *Xenopus* oocyte inside-out patches. (A) The Kv1.3 current was evoked by the step depolarization indicated below the current trace. At the time indicated by the pulse protocol above the trace, the K^+ concentration bathing the internal face of the inside-out patch was rapidly changed from 98 to 49 mM and back to 98 mM (Materials and Methods). Note the rapid current suppression and recovery. The solid line superimposed on the current trace (dots) represents the best-fit exponential function (slow inactivation is taken into account as described in Materials and Methods). (B) Stretched version of the current trace in panel A emphasizing the ON and OFF phases of the response. The gap represents a break in the time base. Note the symmetrical ON and OFF responses along with the corresponding exponential fits. The best-fit time constants were 320 and 330 μs from the ON and OFF phases, respectively. The slight offset between the early and late parts of the trace is caused by slow inactivation. (C) ON and OFF time constants of the solution exchange process (averages from 12 independent patches using the same θ tube that was employed for all the experiments whose results are reported in Figures 2−4).

and exponential nature of the response to the K^+ concentration jump (Figure 1A,B), we modeled the rapid exchange process as a first-order RC filter with a cutoff frequency f_c equal to $(1/2\pi)(3030)$ (482 Hz). Then, using standard procedures (in Origin 7.0), the signal relaxations were deconvoluted (signal/response in the Fourier domain). The raw signal relaxations appeared to be exponential. As expected, the deconvoluted signals were sharper but the relaxations remained exponential (Figures 2−4). Only the time constants of the higher concentration jumps (e.g., from 20 to 40 mM 1-butanol) were significantly reduced by 3−20% upon deconvolution.

The program AGADIR (developed by L. Serrano's laboratory, EMBL, Heidelberg, Germany) was used to model the free energy changes associated with the putative α-helix−random coil equilibrium in the S4−S5 loop. The Shaw2, Kv3.4, Kv3.4-G371I, Shaw2-SK, and Kv3.4-KS sequences used in these calculations were HSSGLKILIQTFRASAKELTL, HFVGLRVLGHTLRASTNEFLL, HFVGLRVLIHTLRASTNEFLL, HSSGLRVLGHTLRASTKELTL, and HFVGLKILIQTFRASANEFLL, respectively. The underlined segments are defined as the S4−S5 loops (13 residues). On the basis of the helix−coil transition theory (*26*, *27*), the AGADIR algorithm uses empirical parameters stored in a database to estimate a set of energy contributions, which accounts for the stability of the α-helix in solution (*26*, *28*). The energy contributions include the intrinsic tendency of amino acids to be in helical dihedral angles, short-range interactions, and long-range electrostatics. AGADIR has accurately predicted the α-helical content of more than 1000 peptides (including more than 200 protein fragments).

CD Spectroscopy. HPLC-purified (>98%) synthetic peptides corresponding to the S4−S5 loop sequences were purchased from Biopeptide (San Diego, CA). CD spectra were recorded for ∼60 μM peptide solutions in 10 mM phosphate buffer (pH 7.0) using the Jasco J810 spectropolarimeter at room temperature in steps of 0.1 nm. Each spectrum was the average of four scans. 2,2,2-Trifluoroethanol (TFE) was added to the peptide solution to promote the α-helical structure (*29*, *30*).

RESULTS

Solution Exchange Time of a Concentration-Clamp Method Applied to Inside-Out Patches. Fast solution exchange at the cytoplasmic side of cell-free membrane patches is limited by the geometry of the membrane in the patch pipet and the unstirred layer at the membrane (*31*−*34*). To determine the "settling time" of the piezoelectric solution exchange system (Materials and Methods), we exposed inside-out patches expressing Kv1.3 currents to an internal K^+ concentration jump (from 98 mM to 49 mM to 98 mM). Limited diffusion caused by the invagination of the membrane patch into the pipet was minimized by forming the pipet−membrane seal in the absence of suction or the presence of slight positive pressure in the patch pipet. A step depolarization from −100 to 50 mV evoked the outward Kv1.3 currents. Large macroscopic Kv1.3 currents in *Xenopus* oocyte macropatches provided an ideal signal-to-noise ratio for an accurate estimation of the solution exchange time (Figure 1). As a result of a change in the driving force for the outward K^+ current and a reduction in single-channel conductance, fast solution switching from 98 to 49 mM (ON) resulted in a fast suppression of the current (to ∼40% of control; Figure 1A). The current was rapidly restored to the expected level (taking into account slow inactivation) upon switching back to 98 mM K^+ (OFF). If we assume that the changes in the driving force and single-channel conductance are instantaneous (in the relevant time scale of our measurements), the time course of current suppression upon rapid reduction of the internal K^+ concentration reflects the solution exchange time of the system. The ON and OFF current responses were complete in ∼1 ms, with a 10−90% change taking place in 800 μs (Figure 1B,C). These results demonstrated that the piezoelectric solution exchange system applied here was suitable for investigating the fast interactions between 1-alkanols and Shaw2 channels on the millisecond time scale.

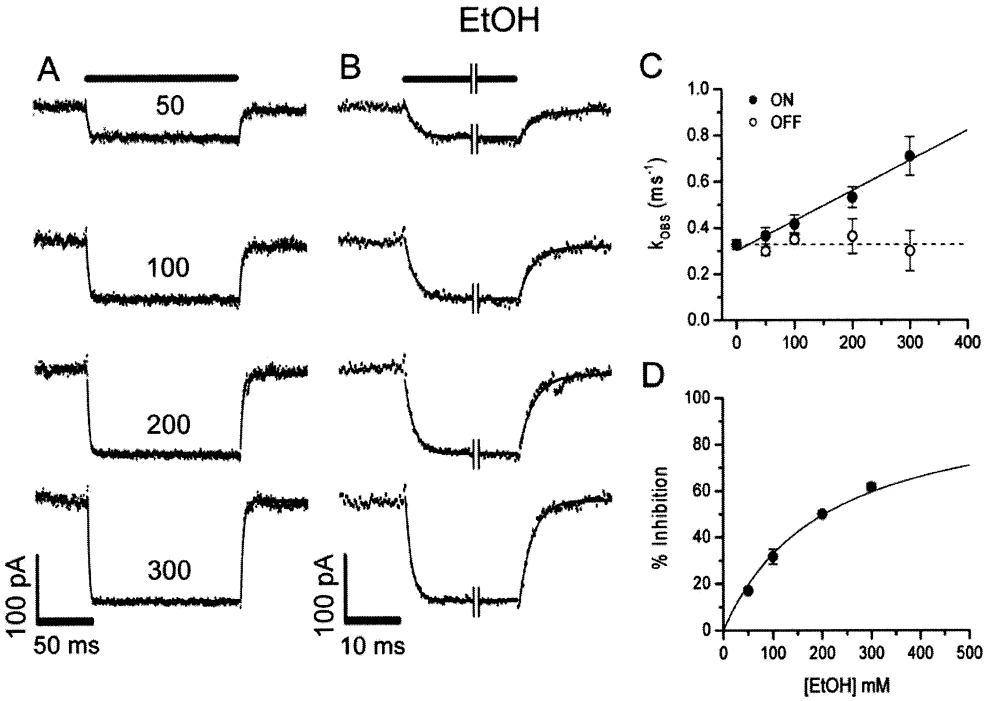

FIGURE 2: Kinetics of the inhibition of Shaw2 K^+ channels by ethanol. (A) Rapid reversible inhibition of Shaw2-F335A currents by the indicated concentrations of ethanol. The current traces were evoked as described in Materials and Methods. Each current trace is the average of 70−100 ON/OFF responses that was deconvoluted as explained in Materials and Methods to correct for the "blurring" effect introduced by the finite exchange time of the concentration-clamp. Smooth solid lines superimposed on the current traces (dots) are the best-fit single exponentials (Materials and Methods) that describe the time course of the inhibition and recovery. (B) Stretched versions of current traces in panel A emphasizing the ON and OFF phases of the signal. The gap indicated by parallel vertical bars represents a break in the time base. Note the fast concentration-dependent ON phase and the slower concentration-independent OFF phase. (C) Observed rates of current inhibition (ON) and recovery (OFF) vs ethanol concentration. The observed rates (k_{obs} = 1/time constant) are derived from the best-fit exponential functions. Note that the ON rate depends on concentration, whereas the OFF rate is independent of concentration (and is always slower than the rate of inhibition). The solid line is the best-fit linear regression with a slope that corresponds to the second-order association rate constant (1.3×10^3 M^{-1} s^{-1}). The dashed horizontal line represents the average value of the observed recovery rate (302 s^{-1}). Note the close agreement between the predicted (*y*-intercept) and measured OFF rates. The estimated dissociation constant ($K_D = k_{OFF}/k_{ON}$) equals 232 mM. (D) Equilibrium dose−inhibition curve derived form the steady-state level of the inhibition observed in panel A (Materials and Methods). The solid line is the best fit assuming the Hill equation ($K_{0.5}$ = 205 mM, n_H = 1.0). All symbols and error bars represent the mean ± the standard error from three independent patches. In some instances, the error bars are smaller than the size of the symbols.

To ensure that the extracted kinetic parameters are not influenced by the filter effect of the finite exchange time of the system, all recorded signals were deconvoluted as explained in Materials and Methods. The deconvoluted current relaxations evoked by different 1-alkanol concentrations were analyzed to extract the binding and unbinding rate constants (Figures 2−4).

The Inhibition of Shaw2 Channels by 1-Alkanols Exhibits Second-Order Kinetics. We compared the effects of ethanol, 1-butanol, and 1-hexanol on Shaw2 K^+ channels to investigate the presence of second-order kinetics and the effect of alkyl chain length on the derived binding kinetics (Figures 2−6). In these experiments, we used the strongly expressing mutant Shaw2-F335A whose electrophysiological properties and 1-alkanol sensitivity are similar to those of the wild-type channel (*24*). Throughout this report, we refer to Shaw2-F335A as Shaw2. The improved expression of the mutant in *Xenopus* oocyte macropatches (Materials and Methods) allowed the high signal-to-noise ratio necessary for a detailed kinetic analysis (Figures 2−4A). Upon fast application and washout of the 1-alkanols tested here, Shaw2 K^+ channels exhibited fast reversible inhibition and the ON and OFF current relaxations evoked by the concentration jumps were described well by assuming an exponential function (Materials and Methods; Figures 2−4B). The relationship between the observed rate constants (k_{obs} = 1/time constant) and concentration revealed similar patterns for the three 1-alkanols studied here (Figures 2C−4C). The observed association rate constants were linearly dependent on concentration, and the dissociation rate constants were concentration-independent (and always slower than the ON phase). If pseudo-first-order conditions are assumed ([ligand] ≫ [receptor]), the kinetics of current inhibition by 1-alkanols applied to the intracellular side of the membrane agree with a second-order mechanism, which supports the presence of a simple ligand−receptor interaction at an internal binding site in the Shaw2 K^+ channel. Relative to the results from 1-alkanols applied to the intracellular side of the membrane, we have previously shown that the observed rate constant of the inhibition by externally applied 1-alkanols is at least 3 orders of magnitude slower (*18*), which supports the presence of an internal site. The second-order association rate constants [derived from the slopes of the linear relationship between the observed association rates and 1-alkanol concentration (Figures 2C−4C)] and the observed dissociation rate constants are summarized in Table 1. In further agreement with the second-order mechanism, the estimations of the dissociation rate constants obtained from the *y*-intercept of the linear regressions and from the exponential relaxations of the OFF signal relaxations were very similar

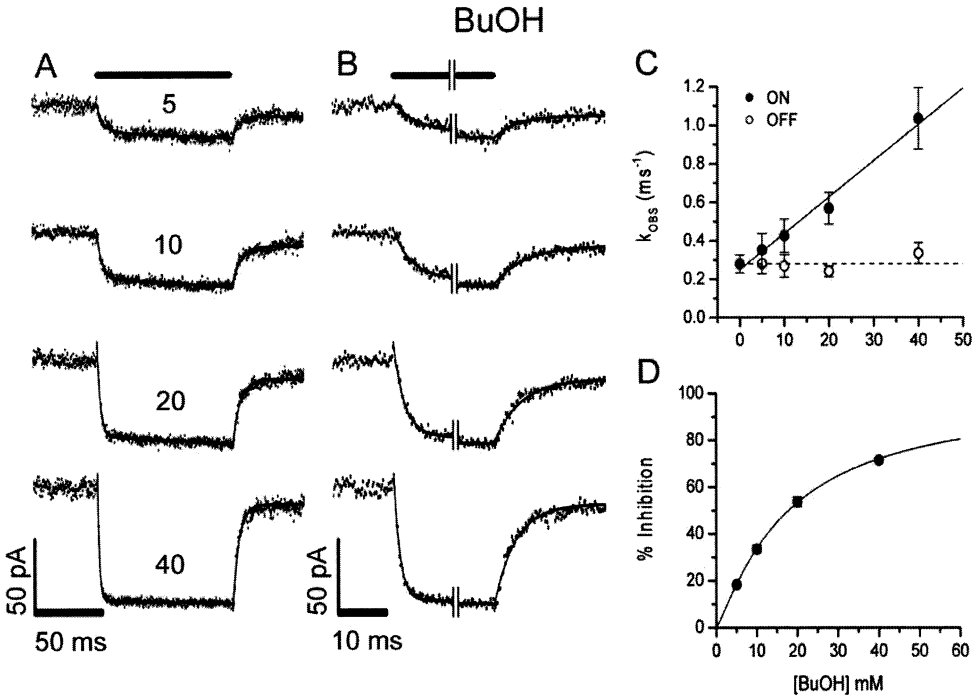

FIGURE 3: Kinetics of the inhibition of Shaw2 K^+ channels by 1-butanol. (A) Rapid reversible inhibition of Shaw2-F335A currents by the indicated concentrations of 1-butanol. Further details of these experiments are as described in the legend of Figure 2. Smooth solid lines superimposed on the current traces (dots) are the best-fit single exponentials (Materials and Methods) that describe the time course of the inhibition and recovery. (B) Stretched versions of current traces in panel A emphasizing the ON and OFF phases of the signal. The gap indicated by parallel vertical bars represents a break in the time base. Note the fast concentration-dependent ON phase and the slower concentration-independent OFF phase. (C) Observed rates of current inhibition (ON) and recovery (OFF) vs 1-butanol concentration. The observed rates (k_{obs} = 1/time constant) are derived from the best-fit exponential functions. Note that the ON rate depends on concentration, whereas the OFF rate is independent of concentration (and is always slower than the rate of inhibition). The solid line is the best-fit linear regression with a slope that corresponds to the second-order association rate constant (1.9×10^4 M^{-1} s^{-1}). The dashed horizontal line represents the average value of the observed recovery rate (250 s^{-1}). Note the close agreement between the predicted (*y*-intercept) and measured OFF rates. The estimated dissociation constant ($K_D = k_{OFF}/k_{ON}$) equals 13 mM. (D) Equilibrium dose−inhibition curve derived form the steady-state level of inhibition observed in panel A (Materials and Methods). The solid line is the best fit assuming the Hill equation ($K_{0.5}$ = 18 mM, n_H = 1.0). All symbols and error bars represent the mean ± the standard error from five independent patches. In some instances, the error bars are smaller than the size of the symbols.

(Figures 2C−4C). The validity of these measurements can also be tested by computing the equilibrium dissociation constants ($K_D = k_{OFF}/k_{ON}$) and comparing these values with those obtained from equilibrium measurements [i.e., the $K_{0.5}$ obtained from the Hill equation analysis of the concentration dependence of the steady-state level of inhibition (Figures 2D−4D)]. We found a good agreement between these estimates (Figures 5 and 6B). Moreover, independent two-electrode voltage-clamp recordings with intact oocytes yielded $K_{0.5}$ values that are similar to those obtained here (*17*, *18*). Overall, the correlation between three independent measurements of the equilibrium dissociation constants for three 1-alkanols is close to unity (Figure 5). Thus, the kinetic analysis provided robust estimates of the rate constants that govern the inhibition of Shaw2 channels by 1-alkanols.

The Second-Order Association Rate Constants Are Exponentially Dependent on the 1-Alkanol Carbon Chain Length. Between ethanol and 1-hexanol, the binding free energy change of 1-alkanols interacting with Shaw2 channels decreases with alkyl chain length (*18*). This relationship agrees with the Meyer−Overton rule, which suggests a hydrophobic site of action. To what extent do hydrophobic interactions control the association and dissociation kinetics of 1-alkanols? What is the role of polar interactions on 1-alkanol binding kinetics? Given the amphiphilic character of 1-alkanols, insights to answer these questions were gained from the kinetic analysis presented above. Clearly, the association rate constant depends steeply on the alkyl chain length, increasing *e*-fold for every carbon atom (Figure 6A and Table 1). In contrast, the dissociation rate constant only decreased ~2-fold from ethanol to 1-hexanol (Figure 6A and Table 1). From this kinetic analysis, the dependence of the binding free energy change on alkyl chain length yielded a slope of −3.2 kJ mol^{-1} carbon $atom^{-1}$ (Figure 6B), which is in excellent agreement with independent equilibrium measurements previously reported (*17*, *18*). As expected, therefore, the binding of 1-alkanols to Shaw2 channels is dominated by a hydrophobic effect. The modest reduction in the dissociation rate constant with alkyl chain length suggests, however, that the lifetime of the alcohol−channel complex ($1/k_{OFF}$ = 3−5 ms) depends on weak dispersion forces involving van der Waals contacts and other critical polar interactions (see the Discussion).

A Correlation between the 1-Alkanol Binding Free Energy Change and the α-Helical Propensity of the S4−S5 Loop in K^+ Channels. Our earlier studies showed that mammalian Kv3.4 channels are 1-alkanol resistant and that the cytoplasmic S4−S5 loop in Shaw2 K^+ channels confers the inhibition by 1-alkanols (*17*, *18*). The latter study also showed that the 1-alkanol resistance of Kv3.4 is independent of the N-type inactivation domain, and that exchange of all seven amino acid differences between the S4−S5 loops of Kv3.4 and

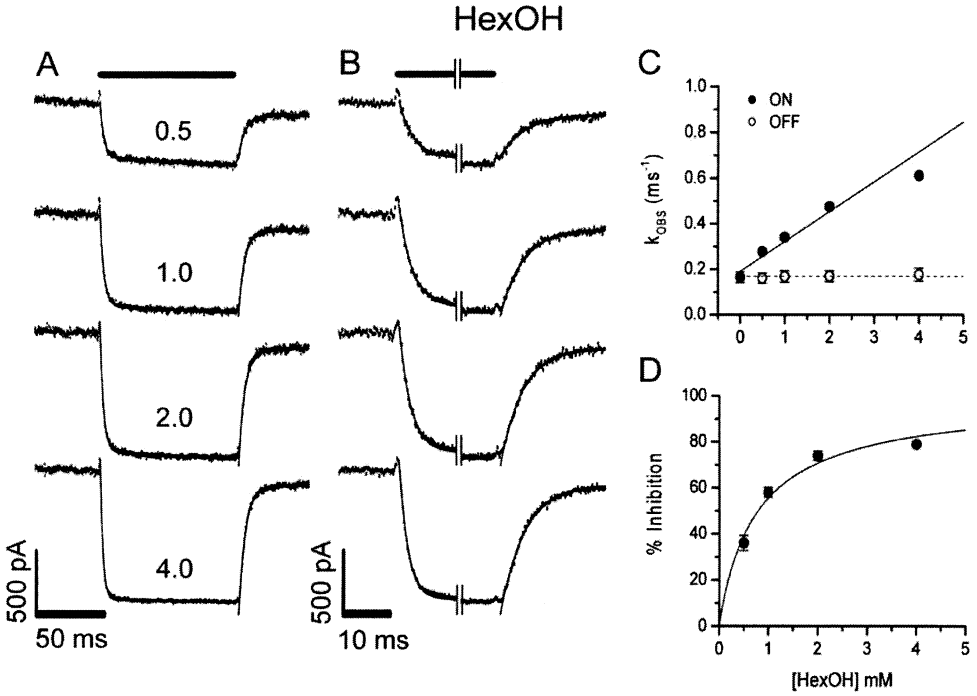

FIGURE 4: Kinetics of the inhibition of Shaw2 K^+ channels by 1-hexanol. (A) Rapid reversible inhibition of Shaw2-F335A currents by the indicated concentrations of 1-hexanol. Further details of these experiments are as described in the legend of Figure 2. Smooth solid lines superimposed on the current traces (dots) are the best-fit single exponentials (Materials and Methods) that describe the time course of the inhibition and recovery. (B) Stretched versions of current traces in panel A emphasizing the ON and OFF phases of the signal. The gap indicated by parallel vertical bars represents a break in the time base. Note the fast concentration-dependent ON phase and the slower concentration-independent OFF phase. (C) Observed rates of current inhibition (ON) and recovery (OFF) vs 1-hexanol concentration. The observed rates (k_{obs} = 1/time constant) are derived from the best-fit exponential functions. Note that the ON rate depends on concentration, whereas the OFF rate is independent of concentration (and is always slower than the rate of inhibition). The solid line is the best-fit linear regression with a slope that corresponds to the second-order association rate constant (1.3×10^5 M^{-1} s^{-1}). The dashed horizontal line represents the average value of the observed recovery rate (191 s^{-1}). Note the close agreement between the predicted (*y*-intercept) and measured OFF rates. The estimated dissociation constant ($K_D = k_{OFF}/k_{ON}$) equals 1.5 mM. (D) Equilibrium dose−inhibition curve derived form the steady-state level of inhibition observed in panel A (Materials and Methods). The solid line is the best fit assuming the Hill equation ($K_{0.5}$ = 0.8 mM, n_H = 1). All symbols and error bars represent the mean ± the standard error from four independent patches. In some instances, the error bars are smaller than the size of the symbols.

Shaw2 K^+ channels was sufficient to exchange the sensitivities of these channels to 1-alkanols. We hypothesized that the differential α-helical propensities of the corresponding S4−S5 loops in Shaw2 and Kv3.4 channels may explain their distinct sensitivities to 1-alkanols. To test the viability of this hypothesis, Table 2 compares the measured 1-butanol binding free energy changes (ΔG_B) of several K^+ channels and the theoretical free energy change of the α-helix−coil equilibrium (ΔG_H) for the S4−S5 loop of the corresponding K^+ channels (Shaw2, Kv3.4, and the corresponding mutants). The ΔG_B values were computed from previously published estimates of the apparent equilibrium constants (*18*). The ΔG_H (computed as explained in Materials and Methods) reflects the α-helical propensity of the S4−S5 loop. According to the hypothesis, the ΔG_H of the Shaw2 sequence was smaller than that of Kv3.4 by ∼2 kcal/mol, which suggests that the S4−S5 loop of Shaw2 is more likely to adopt the α-helical structure. When the S4−S5 sequences were exchanged between Shaw2 and Kv3.4 [Shaw2-SK is Shaw2 hosting the Kv3.4 S4−S5 linker, and Kv3.4-KS is Kv3.4 hosting the Shaw2 S4−S5 linker (*18*)], the ΔG_H increases for Shaw2 (from 8.5 to 11.7 kcal/mol) and decreases for Kv3.4 (from 10.7 to 7.4 kcal/mol). Furthermore, even a single mutation that confers significant 1-butanol inhibition in Kv3.4 (Kv3.4-G371I) by increasing the 1-butanol binding free energy change ($\Delta\Delta G_B \sim 0.4$ kcal/mol; Table 2) also increases the theoretical α-helical propensity (i.e., ΔG_H decreases).

To probe more directly the secondary structure of the S4−S5 loop, we applied CD spectroscopy to investigate synthetic peptides corresponding to the loop sequences of Shaw2, Kv3.4, and Kv3.4-G371I (Materials and Methods). The spectra from the Shaw2 and Kv3.4 peptides yielded strikingly different profiles (Figure 7A). While the Shaw2 peptide exhibited features that are consistent with the presence of secondary structure (α-helix and β sheet), the Kv3.4 peptides appeared to be largely random coil. Then, we tested the α-helical propensities of these peptides by examining their response to increasing concentrations of an agent that promotes the α-helical structure [2,2,2-trifluoroethanol (TFE); Figure 7B−D (*29*, *30*)]. Clearly (and in agreement with the calculations presented above), the Shaw2 peptide readily adopted the α-helical structure as shown by the significantly increased ellipticity at 220 nm with concentrations of TFE as low as 10−20% (Figure 7D). In contrast, the Kv3.4 peptide was significantly more resistant to adoption of the α-helical structure because it exhibited a more gradual increase in ellipticity at 220 nm (Figure 7D). Notably, the ellipticity of the Kv3.4 peptide only reached the level of the Shaw2 peptide at the highest concentration of TFE (90%). Shaw2 and Kv3.4 peptides appeared to be mostly α-helical in the presence of high TFE concentrations, which agrees

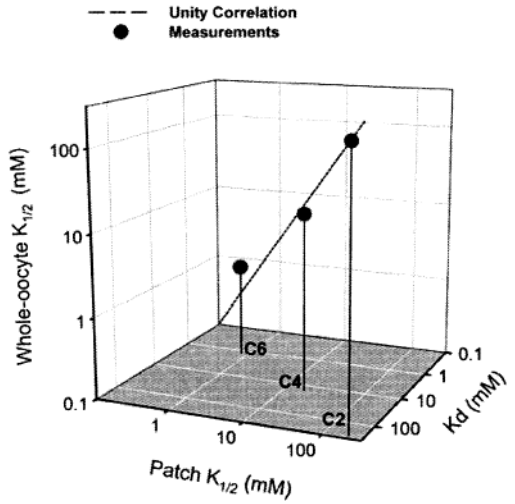

FIGURE 5: Correlation between three independent determinations of the equilibrium dissociation constants for the interaction of 1-alkanols with Shaw2 K^+ channels. The three-dimensional plot simultaneously compares K_D (k_{OFF}/k_{ON}, from Table 1) and two estimates of the equilibrium dissociation constants ($K_{0.5}$-patch and $K_{0.5}$-whole oocyte) obtained from (1) the analysis of the steady-state level of inhibition in Figures 2−4 (i.e., the same experiments that were used to determine the rate constants) and (2) the previously published analysis of the steady-state level of inhibition in intact oocytes expressing Shaw2 channels (*17*, *18*). C2, C4, and C6 correspond to ethanol, 1-butanol, and 1-hexanol, respectively. The dashed line corresponds to a unity correlation, which demonstrates the close agreement between the three measurements.

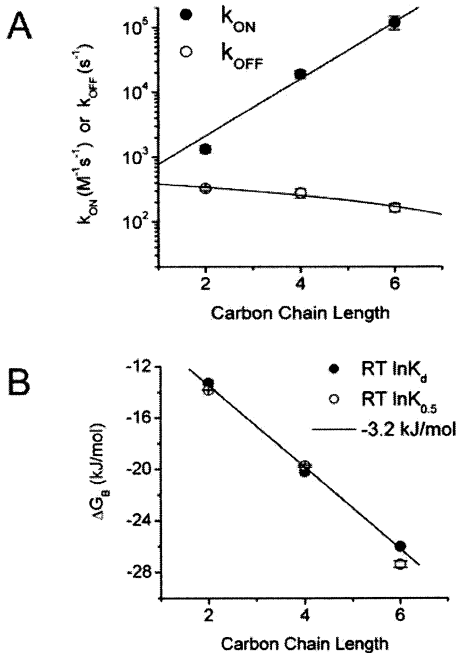

FIGURE 6: Effect of carbon chain length on the kinetic parameters of the inhibition of Shaw2 K^+ channels by 1-alkanols. (A) Relationship between k_{ON} or k_{OFF} and the carbon chain length of 1-alkanols. k_{ON} depends exponentially on chain length. The solid line through the filled symbols represents the best-fit exponential growth function. k_{ON} increases *e*-fold per carbon atom. The solid line through the empty symbols represents the best-fit linear regression. k_{OFF} decreases at a rate of 42 s^{-1} per carbon. Between ethanol and 1-hexanol, k_{OFF} decreases ~2-fold. (B) Relationship between the binding free energy change ($\Delta G_B = RT \ln K$, where R is the gas constant, T is the absolute temperature, and K is the equilibrium dissociation constant) and the carbon chain length of 1-alkanols. K_D and $K_{0.5}$ are estimated as explained in text. Equilibrium constants are expressed in unitary mole fraction units. The solid line through the symbols represents the best-fit linear regression with the slope indicated in the plot.

with the results of a recent study that investigated the NMR-based structure of the S4−S5 loop in Shaker K^+ channels (*20*). The mutant peptide Kv3.4-G371I exhibited a novel intermediate behavior. It responded readily to low TFE concentrations and approached the response of the Shaw2 peptide in a manner that was clearly distinct from the response of the wild-type Kv3.4 peptide. This intermediate behavior correlates with the intermediate inhibition of the Kv3.4-G371I channels by 1-alkanols (Table 2; cf. ref *9*). Thus, the theoretical computations and experimental results presented above suggest that the S4−S5 loops of Shaw2 and Kv3.4 channels may adopt distinct secondary structures that can explain their differential interaction with 1-alkanols, and the interactions that control the internal activation gate (see the Discussion).

DISCUSSION

We have applied kinetic analysis and CD spectroscopy to investigate the molecular features of a 1-alkanol binding site in the Shaw2 K^+ channel. The kinetic analysis employed a fast solution exchange method with a settling time of ~1 ms, which allowed accurate estimation of the binding and unbinding rate constants of 1-alkanols (ethanol, 1-butanol, and 1-hexanol) to infer the presence of amphiphilic interactions. The α-helical propensity of the S4−S5 loop in the pore-forming subunit was also investigated to test the relationship between the binding free energy change of 1-alkanols and the presence of secondary structure in that region. This feature may be critical for 1-alkanol binding and/or the allosteric inhibition of channel gating by 1-alkanols.

A Simple Ligand−Receptor Interaction at an Amphiphilic Site Underlies the Inhibition of Shaw2 K^+ Channels by 1-Alkanols. As the most economical interpretation, the concentration dependence of the observed rate constants strongly suggests a second-order mechanism for the reversible interaction of 1-alkanols (A) with the Shaw2 K^+ channel (C) at an internal site (Scheme 1).

Table 1: Kinetic Parameters of the Inhibition of Shaw2 Channels by 1-Alkanols

1-alkanol	k_{ON}[a] (M^{-1} s^{-1})	k_{OFF}[b] (s^{-1})	N[c]
ethanol	$(1.3 \pm 0.2) \times 10^3$	329 ± 21	3
1-butanol	$(1.9 \pm 0.3) \times 10^4$	280 ± 47	5
1-hexanol	$(1.2 \pm 0.3) \times 10^5$	165 ± 24	4

[a] Obtained from the slope of the relationship between the observed ON rate and the 1-alkanol concentration (Figures 2−4). [b] Obtained from the average value of the concentration-independent OFF rates observed at different concentrations (Figures 2−4). This value was in excellent agreement with the *y*-intercept of the linear regression that describes the relationship between the observed ON rate and the 1-alkanol concentration (Figures 2−4). [c] Number of independent determinations.

Scheme 1

$$A + C \underset{k_{OFF}}{\overset{k_{ON}[A]}{\rightleftharpoons}} AC$$

The apparent asymmetry between the effects of alkyl chain length on the association and dissociation rate constants is,

Table 2: Energetics of the Inhibition of Shaw-Related K^+ Channels by 1-Butanol and the α-Helical Propensity of the S4−S5 Loop

K^+ channel	K_i[a] (mM)	ΔG_B[b] (kcal/mol)	$\Delta\Delta G_B$[c] (kcal/mol)	ΔG_H[d] (kcal/mol)	$\Delta\Delta G_H$[e] (kcal/mol)
Shaw2	17	−2.40	0	8.5	0
Kv3.4	70	−1.57	0	10.7	0
Shaw2-SK	63	−1.63	−0.77	11.7	−3.2
Kv3.4-G371I	39	−1.91	0.35	9	1.7
Kv3.4-KS	10	−2.71	1.14	7.4	3.3

[a] Apparent equilibrium dissociation constants obtained from 1-butanol dose−inhibition curves as described previously (*17*, *18*). [b] Gibbs free energy changes for 1-butanol inhibition ($\Delta G = RT \ln K_i$, where R and T are the universal gas constant and the absolute temperature, respectively). [c] Difference between binding free energy changes of the mutants relative to that of the wild type ($\Delta\Delta G_B = \Delta G_{BWT} - \Delta G_{BMUT}$). [d] Theoretical Gibbs free energy changes of the helix−coil equilibrium in the S4−S5 loop (Materials and Methods). [e] Difference between the calculated helix−coil free energy changes of the mutants relative to that of the wild type ($\Delta\Delta G_H = \Delta G_{HWT} - \Delta G_{HMUT}$).

however, intriguing (Figure 6A). A more symmetric pattern is expected if we assume that both binding and unbinding mainly depend on hydrophobic interactions. To understand the observed asymmetry, we need to examine more closely the mechanism that may underlie the binding of 1-alkanols to the Shaw2 protein. Clearly, the observed second-order association rate constants (Table 1) are 4−6 orders of magnitude slower than the value expected for a diffusion-controlled process (~10^9 M^{-1} s^{-1}). This difference indicates that encounters between the channel and 1-alkanols rarely result in productive collisions, which is the expected behavior of partially diffusion-controlled bimolecular reactions that are commonly found in biological systems (*35*). The association rate constants in the cases studied here are especially slower because the putative 1-alkanol binding site is not a surface-exposed interfacial pocket (*5*, *12*). More likely, this binding site is a preformed hydrophobic crevice or packing defect (protein−protein or lipid−protein) where 1-alkanols may need some time to find stable interactions. Also, the binding site may undergo conformational adaptive changes that control the binding. Thus, a more explicit scheme for explaining the binding of 1-alkanols to Shaw2 K^+ channels (and probably other proteins too) must include an encounter complex (A···C) in equilibrium with the free reactants (A + C) and the bound state (AC) as shown below (*35*):

Scheme 2

$$A + C \underset{k_{-1}}{\overset{k_{+1}}{\rightleftharpoons}} A\cdots C \underset{k_{-2}}{\overset{k_{+2}}{\rightleftharpoons}} AC$$

This scheme assumes that an intermediate encounter complex forms before stable interactions are established between the channel and the alcohol to produce the bound state. Inhibition of the channel is only associated with the bound state. The contribution of an encounter complex has been also evoked to explain the severe asymmetry of the effect of charge substitutions on the association and dissociation rate constants that govern binding of a scorpion toxin to the Shaker K^+ channel (*36*). For 1-alkanols, formation of the encounter complex may represent the rapid partition of the alcohol in a hydrophobic cavity, which depends on diffusion and is dominated by a hydrophobic effect. In the encounter complex, the alcohol seeks favorable contacts and interactions as it jiggles in the hydrophobic cavity. Eventually, the bound state is reached when stable van der Waals contacts and a hydrogen bond are finally formed (*5*, *12*, *15*). More frequently, however, the alcohol is not stabilized in the cavity and falls off (i.e., productive collisions are rare); then, it quickly re-enters the cavity to make another attempt. If we assume the steady-state approximation for the concentration of the encounter complex (*35*), the following equations define the observed forward and backward rates (k_F and k_B, respectively) for Scheme 2:

$$k_F = k_{+1}\left(\frac{k_{+2}}{k_{+2} + k_{-1}}\right) \quad (1)$$

and

$$k_B = k_{-2}\left(\frac{k_{-1}}{k_{+2} + k_{-1}}\right) \quad (2)$$

We can simplify these equations by assuming that the formation of the bound state is the rate-limiting step of the reaction, as explained above (i.e., productive collisions are rare). In this case, $k_{+2} \ll k_{-1}$ (in contrast to a reaction operating near the diffusion-controlled limit where $k_{+2} \gg k_{-1}$). Accordingly, the simplified definitions of k_F and k_B are

$$k_F = k_{+1}\left(\frac{k_{+2}}{k_{-1}}\right) \quad (3)$$

and

$$k_B = k_{-2} \quad (4)$$

Then, it is more clearly apparent that k_F depends on the hydrophobic effect that controls the partitioning of the alcohol in the binding cavity and the rate-limiting formation of the bound state, which is governed by k_{+2} (eq 3). The structural bases of the rate-limiting step are probably complex, but are likely to include a combination of two possible scenarios: (1) the alcohol seeks stable interactions in a pre-existing cavity, and (2) the protein undergoes local adaptive structural changes as the alcohol attempts to establish stable interactions in a cavity. Local adaptive changes upon ligand binding in a hydrophobic pocket have been clearly demonstrated by others (*37*). In both cases, the size of the alkyl chain is likely to play an important favorable role. Therefore, the observed association rate constant depends steeply on alkyl chain length. We can also see that k_B is the rate constant that governs the breakdown of the bound state (eq 4). If, in addition to van der Waals interactions involving the alkyl chain, the stability of a hydrogen bond is the dominant factor that limits the dissociation of the alcohol from its binding site, the dissociation rate constant may not strongly depend on alkyl chain length, as we observed. The hydroxyl group of 1-alkanols is a good hydrogen bond donor that is likely to form a stable hydrogen bond with the backbone of the polypeptide or the side chain group of polar amino acids (*15*). As suggested by others (*12*), we can then hypothesize that the free energy change of 1-alkanol binding to the Shaw2 K^+ channel depends on a positive entropy change and a

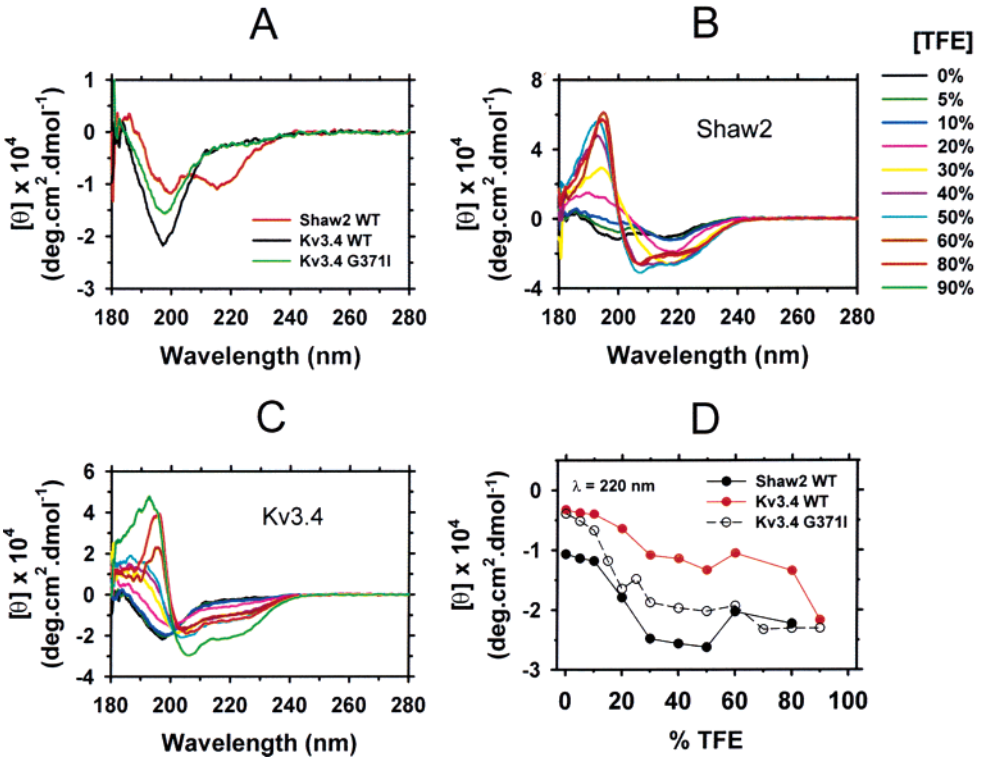

FIGURE 7: CD spectroscopy of synthetic peptides corresponding to the S4−S5 loop of Shaw2 and Kv3.4 K^+ channels. (A) Overlaid CD spectra recorded in the absence of TFE. The 13-mer peptide sequences are given in Materials and Methods (underlined). Note that the spectra from the Kv3.4 and Kv3.4-G371I peptides correspond to the random-coil profile, whereas the spectrum from the Shaw2 peptide is more consistent with the presence of secondary structure. (B and C) CD spectra recorded in the presence of increasing concentrations of TFE (from 5 to 90%). Color-coded lines on the right-hand side of the graph in panel B denote the corresponding concentrations of TFE. (D) Ellipticity (θ) at 220 nm vs TFE concentration. Each curve was generated from two independent measurements. Note the relatively sensitive and resistant responses of the Shaw2 and Kv3.4 peptides, respectively. The response of the Kv3.4-G371I peptide appears to be intermediate.

negative enthalpy change. The former results from the hydrophobic effect that drives the 1-alkanol to the binding site, and the latter represents the energetic cost of establishing stable weak electrostatic interactions in the binding site (van der Waals interactions and a hydrogen bond). Further studies that examine the temperature dependence of rate constants are necessary to test this hypothesis.

Shedding Light on the Structural Basis of the Inhibition of Shaw2 K^+ Channels by 1-Alkanols. Exchanging the S4−S5 loop between Kv3.4 and Shaw2 subunits is sufficient to confer or drastically inhibit the inhibition by 1-alkanols (*18*; Table 2). Interestingly, the crystal structure of a bacterial Kv subunit (KvAP) reveals the S4−S5 loop as the tip of a long α-helix that constitutes the S5 segment (*19*). We hypothesize that the very distinct α-helical propensity of peptides corresponding to the S4−S5 loops of Shaw2 and Kv3.4 channels (Table 2 and Figure 7) provides a feasible explanation for their distinct sensitivities to 1-alkanols. For instance, the α-helical structure in the Shaw2 S4−S5 loop may be necessary to maintain the amphiphilic cleft that constitutes the 1-alkanol binding site. This cleft is less likely to exist in Kv3.4 channels because the S4−S5 loop exhibits a reduced α-helical propensity. The crystal structure of a KvAP channel also demonstrates that the S4−S5 loop is indeed cytoplasmic. Thus, if the S4−S5 loop contributes to the 1-alkanol binding site in Shaw2 channels, it can be directly reached from the internal aqueous compartment. The relatively rapid second-order kinetics and the slope of the relationship between the binding free energy change and the alkyl chain length (Figures 2−5) are consistent with an apparently direct internal access to the amphiphilic 1-alkanol binding site in Shaw2 channels.

The structurally distinct S4−S5 loops of Shaw2 and Kv3.4 may also contribute to the activation gating differences between these channels. A less structured S4−S5 loop in Kv3.4 channels may confer the necessary flexibility to allow channel activation tightly coupled to the movement of the S4 voltage sensor. In contrast, activation of Shaw2 K^+ channels mainly occurs as a first-order concerted transition, which is not tightly coupled to the voltage sensor. This concerted transition might correspond to the main late opening step in Kv channels (*38*). The control of the internal activation gate without a significant influence by the voltage sensor could be the result of a more structured S4−S5 loop in Shaw2 K^+ channels. Also, the movement of a voltage sensor is less likely to contribute to the Shaw2 activation because the first two critical arginines (conserved in Kv3.4 and other Kv channels) and the last lysine of the Shaker S4 segment are absent in Shaw2 K^+ channels (*39*). In light of these considerations, it is alternatively possible that the distinct α-helical propensities of the S4−S5 loops may also influence the allosteric coupling between activation gating and the binding of 1-alkanols.

CONCLUSION

Amphiphilic binding sites are the foundation of the protein-based theories of alcohol intoxication and general anesthesia that have gained significant recognition in the past decade

(*1*−*6*). The physiological importance and molecular properties of such sites have been mainly inferred from the relationship between the narcotic effect and anesthetic solubility, studies with model soluble proteins, and theoretical arguments (*5*, *9*, *12*−*15*). Although it is clear that ion channels and other membrane proteins harbor relatively specific and relevant sites for general anesthetic agents (*1*−*6*), the physicochemical and molecular features of these sites are not well-understood. The observations presented here support the presence of amphiphilic interactions that mediate the inhibition of the neuronal Shaw2 K^+ channel by 1-alkanols at a discrete binding site. Moreover, the α-helical propensity of the S4−S5 loop in the pore-forming Shaw2 subunit is likely to play a key role in the binding of 1-alkanols and/or the allosteric modulation of the Shaw2 K^+ channel by 1-alkanols.

ACKNOWLEDGMENT

We thank Drs. Donard S. Dwyer and Jonas S. Johansson for critically reading this manuscript. Also, we thank Ms. Carmen Rocha and Mr. Andrew Graber for harvesting high-quality *Xenopus* oocytes.

REFERENCES

1. Peoples, R. W., Li, C., and Weight, F. F. (1996) *Annu. Rev. Pharmacol. Toxicol. 36*, 185−201.
2. Diamond, I., and Gordon, A. S. (1997) *Physiol. Rev. 77*, 1−20.
3. Harris, R. A. (1999) *Alcohol Clin. Exp. Res. 23*, 1563−1570.
4. Yamakura, T., Bertaccini, E., Trudell, J. R., and Harris, R. A. (2001) *Annu. Rev. Pharmacol. Toxicol. 41*, 23−51.
5. Miller, K. W. (2002) *Br. J. Anaesth. 89*, 17−31.
6. Urban, B. W. (2002) *Br. J. Anaesth. 89*, 167−183.
7. Franks, N. P., and Lieb, W. R. (1985) *Nature 316*, 349−351.
8. Alifimoff, J. K., Firestone, L. L., and Miller, K. W. (1989) *Br. J. Pharmacol. 96*, 9−16.
9. Moss, G. W., Curry, S., Franks, N. P., and Lieb, W. R. (1991) *Biochemistry 30*, 10551−10557.
10. Mascia, M. P., Trudell, J. R., and Harris, R. A. (2000) *Proc. Natl. Acad. Sci. U.S.A. 97*, 9305−9310.
11. Zhang, Y., Trudell, J. R., Mascia, M. P., Laster, M. J., Gong, D. H., Harris, R. A., and Eger, E. I. (2000) *Anesth. Analg. (Baltimore) 91*, 1294−1299.
12. Eckenhoff, R. G., and Johansson, J. S. (1997) *Pharmacol. Rev. 49*, 343−367.
13. Eckenhoff, R. G., Petersen, C. E., Ha, C. E., and Bhagavan, N. V. (2000) *J. Biol. Chem. 275*, 30439−30444.
14. Trudell, J. R., and Bertaccini, E. (2002) *Br. J. Anaesth. 89*, 32−40.
15. Dwyer, D. S., and Bradley, R. (2000) *Cell. Mol. Life Sci. 57*, 265−275.
16. Covarrubias, M., and Rubin, E. (1993) *Proc. Natl. Acad. Sci. U.S.A. 90*, 6957−6960.
17. Covarrubias, M., Vyas, T. B., Escobar, L., and Wei, A. (1995) *J. Biol. Chem. 270*, 19408−19416.
18. Harris, T., Shahidullah, M., Ellingson, J. S., and Covarrubias, M. (2000) *J. Biol. Chem. 275*, 4928−4936.
19. Jiang, Y., Lee, A., Chen, J., Ruta, V., Cadene, M., Chait, B. T., and MacKinnon, R. (2003) *Nature 423*, 33−41.
20. Ohlenschlager, O., Hojo, H., Ramachandran, R., Gorlach, M., and Haris, P. I. (2002) *Biophys. J. 82*, 2995−3002.
21. Tanford, C. (1973) *The Hydrophobic Effect*, Wiley-Interscience, New York.
22. Haydon, D. A., and Urban, B. W. (1983) *J. Physiol. 341*, 411−427.
23. Beck, E. J., Sorensen, R. G., Slater, S. J., and Covarrubias, M. (1998) *J. Gen. Physiol. 112*, 71−84.
24. Harris, T., Graber, A., and Covarrubias, M. (2003) *Am. J. Physiol.* (in press).
25. Jerng, H. H., Shahidullah, M., and Covarrubias, M. (1999) *J. Gen. Physiol. 113*, 641−660.
26. Muñoz, V., and Serrano, L. (1995) *Curr. Opin. Biotechnol. 6*, 382−386.
27. Muñoz, V., and Serrano, L. (1994) *Nat. Struct. Biol. 1*, 399−409.
28. Lacroix, E., Viguera, A. R., and Serrano, L. (1998) *J. Mol. Biol. 284*, 173−191.
29. Jasanoff, A., and Fersht, A. R. (1994) *Biochemistry 33*, 2129−2135.
30. Sonnichsen, F. D., Van Eyk, J. E., Hodges, R. S., and Sykes, B. D. (1992) *Biochemistry 31*, 8790−8798.
31. Brett, R. S., Dilger, J. P., Adams, P. R., and Lancaster, B. (1986) *Biophys. J. 50*, 987−992.
32. Maconochie, D. J., and Knight, D. E. (1989) *Pfluegers Arch. 414*, 589−596.
33. Cannell, M. B., and Nichols, C. G. (1991) *Biophys. J. 60*, 1156−1163.
34. Sachs, F. (1999) *Biophys. J. 77*, 682−690.
35. Shoup, D., and Szabo, A. (1982) *Biophys. J. 40*, 33−39.
36. Escobar, L., Root, M. J., and MacKinnon, R. (1993) *Biochemistry 32*, 6982−6987.
37. Arkin, M. R., Randal, M., DeLano, W. L., Hyde, J., Luong, T. N., Oslob, J. D., Raphael, D. R., Taylor, L., Wang, J., McDowell, R. S., Wells, J. A., and Braisted, A. C. (2003) *Proc. Natl. Acad. Sci. U.S.A. 100*, 1603−1608.
38. Ledwell, J. L., and Aldrich, R. W. (1999) *J. Gen. Physiol. 113*, 389−414.
39. Smith-Maxwell, C. J., Ledwell, J. L., and Aldrich, R. W. (1998) *J. Gen. Physiol. 111*, 399−420.

BI034738F